Proceedings World Geothermal Congress 2005
Antalya, Turkey, 24-29 April 2005

Pressure Dependent Hydraulic Flow, Heat Transport and Geo-thermo-mechanical Deformation in HDR Crystalline Geothermal Systems: Preliminary Application to Identify Energy Recovery Schemes at Urach Spa

C. I. M[c]Dermott[1], A. L. Randriamanjatosoa[1], H. Tenzer[2] , M. Sauter[3], O. Kolditz[1]

[1]Center for Applied Geoscience, Chair of GeoSystems Research, University of Tübingen, 72076 Tübingen, Germany

[2]ErdwärmeforschungStadtwerke Bad Urach Marktplatz 8, 972574 Bad Urach, Germany

[3]Geoscientific Center, Georg-August University of Göttingen, Goldschmidtstr. 3, 37077 Göttingen, Germany.

e-mail: chris.mcdermott@uni-tuebingen.de

Keywords: Reservoir, Modeling, Finite-element method, HTM, Heat Flow, Geomechanics, Optimization

ABSTRACT

Understanding flow and heat transport pressure and temperature dependent parameters of crystalline rock coupled with geomechanical deformation is particularly important in crystalline geothermal reservoirs. The permeability of these reservoirs is dominated by the fracture systems found within them. In-situ stress conditions have a significant impact on the flow, transport and exchange characteristics of the three dimensional fracture networks. Hydraulic, Thermal and Mechanical coupling (HTM) occurs as a result of the extraction of heat from the reservoirs utilizing high pressure injection and extraction of in situ geofluids. These coupled processes significantly effect the characteristics of heat extraction from the geothermal reservoir.

Based on a newly developed and experimentally calibrated geomechanical model, the changes in the flow and transport parameters within crystalline fractures due to changes in local effective stress as a result of the reservoir fluid draw down, water injection and thermal stresses can be estimated. Using a finite element model of the Bad Urach (South West Germany) potential Hot Dry Rock (HDR) geothermal reservoir comprising tetrahedral elements, this mechanical deformation and alteration of fracture parameters is coupled with state of the art fluid parameter functions dependent on pressure, temperature and salinity for heat capacity, conductivity, viscosity and density. The effects of HTM coupled flow and heat extraction on the reservoir characteristics are investigated to assist in the identification of heat recovery schemes for the long term economical operation of the HDR plant.

1. INTRODUCTION

Geothermal reservoirs are characterized by a complex interaction of several coupled processes. Understanding the processes, their inter-relationships and effects forms the key to the successful investigation and modeling of heat energy extraction e.g. Tsang (1991), O'Sullivan et al. (2001).

Several different modeling approaches to geothermal reservoirs have been undertaken to gain a better understanding of geothermal reservoirs behavior, and to improve the existing models. This is illustrated in a state of the art review by O'Sullivan et al. (2001) and by Sanyal et al. (2000). Examples of such case studies include Rosemanowes Kolditz and Clauser (1998) and Soultz-Sous-Forêts Hot Dry Rock (HDR) investigations in Kolditz (2001), Kolditz (2002), pressure dependent permeability and storage of fracture shear zones McDermott and Kolditz (2004), numerical study on heat extraction from supercritical geothermal reservoirs by Watanabe et al. (2000), and reducing cost and environmental impact of geothermal power through modeling of chemical processes in the reservoir by Pham et al. (2001).

Often due to the number of different parameters involved, e.g. geometry, stress, non linear flow, the only viable approach to modeling is to employ numerical methods Huyakorn and Pinder (1983), Diersch (1985), Helmig (1997), Kolditz (2002).

The HDR technique involves the construction of two boreholes as illustrated in Figures 1 & 2, with the extraction of hot fluids from one borehole, the surface removal of the heat energy for conversion into electricity, and then the subsequent re-injection of the cooled fluids. Modeling this in a reservoir situation involves a geological, hydrogeological and engineering understanding of the processes and difficulties involved.

In this paper we present rock stress, fluid pressure, temperature and salinity dependent modeling tools to assist in the identification of optimal heat recovery schemes for long term economical operation of the Bad Urach (South West Germany) potential Hot Dry Rock (HDR) geothermal reservoir. We approach the HTM coupling from two perspectives

- The mechanical deformation of the fractures under changing effective stress is predicted using a newly developed and experimentally calibrated Geomechanical model. The effective stress is a function of both the hydraulic pressure and thermal stress developed as a result of rock cooling.

- The pressure, temperature and salinity dependent fluid parameters for heat capacity, conductivity, viscosity and density. Based on a substantial literature search state of the art fluid parameters functions are presented.

To model the system, seismic information gained during hydraulic stimulation tests in the crystalline reservoir rocks at a depth of 4000m Baisch et al. (2004) has been used to define the three dimensional geometry of a zone of enhanced permeability. This zone of enhanced permeability is taken to be the Hot Dry Rock natural heat exchanger. It is modeled applying tetrahedral elements within the object orientated finite element program GeoSys/RockFlow. The effects of HTM coupled flow and heat extraction on the

reservoir characteristics are investigated to assist in the identification of optimal heat recovery schemes for the long term economical operation of the HDR plant.

Initial modeling results of the predictive behavior of the reservoir show that the consideration of both the hard rock and fluid HTM dependent parameters is vital for a more reliable investigation of the long term reservoir characteristics, heat extraction possibilities and cooling profile of the reservoir.

2. RESERVOIR GEOMETRY & PARAMETERS

Much research into the potential geothermal usage and HDR concept applied to Bad Urach Tenzer et al. (2002) has been undertaken. Particularly a book edited by Haenel (1982) presents some 43 different scientific papers covering a large amount of fields regarding the reservoir, heat anomaly and geology. Recently hydraulic stimulation has been undertaken in Urach Baisch et al. (2004) to determine the geometrical size of the reservoir and to increase the hydraulic conductivity of the system. Consultants Q-con provided a detailed investigation into the hydraulic parameters of the reservoir Q-con (2003). Most recently Sauter et al. (2004) have undertaken tracer push pull tests to characterize the nature of the fractures within the system.

The above information provided a basis for the construction of a three dimensional model of the reservoir system and estimation of the parameters relevant for flow and transport. The geometry of the reservoir is based upon the geoseismic results interpreted by Baisch et al. (2004), an interpretation of which is shown in Figure 1.

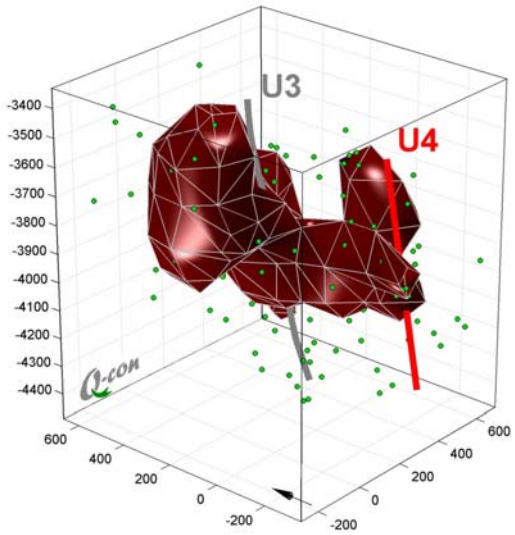

Figure 1: Predicted extent of the enhanced permeability zone for HDR in Urach (Q-con 2003)

The potential natural heat exchanger is found to have a geometry of some 300m height by 300m width by 800m length. The proposed borehole positions maintain a distance of some 400m apart. Figure 2 presents the area chosen for the development of the current model to integrate the THM characteristics. Here as a first estimation referring to Figure 1, a dipole flow circulation between wells U3 and U4 was assumed, limiting the hydraulically relevant areas and allowing us to represent the reservoir geometrically as an ellipsoid. The in situ rock is assumed to have a temperature of 147°C Tenzer et al. (2002) and the injected fluid a down hole temperature of 50°C.

The characteristic element length of the model is around 20m, some 6500 nodes and over 36000 elements are required to represent the reservoir structure. Due to consideration of variable fluid and mechanical characteristics, and the required injection and extraction pressures, model stability required time steps of under 12 hours. Transient flow conditions exist throughout the modelling, due to the HTM coupling.

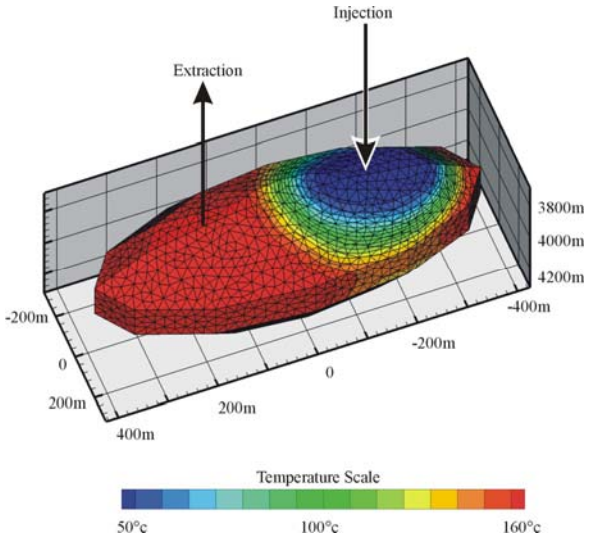

Figure 2: Reservoir Geometry, (Heat distribution after 20 years of operation. Average 13l/s at 10MPa injection and –10MPa extraction pressure)

3. SIMULATION OF HEAT EXTRACTION USING THE HDR TECHNIQUE

3.1 Simulation

Simulation of heat extraction from the reservoir rock during HDR application by applying the finite element technique is possible by considering the two dominant processes involved. That is firstly the hydraulic flow and secondly the heat flow. The equations describing hydraulic flow Freeze and Cherry (1979) based on the mass balance, can be expressed as

$$S\frac{\partial p}{\partial t}-\frac{\partial}{\partial x_\alpha}\left(\frac{k_{\alpha\beta}}{\mu}\left(\frac{\partial p}{\partial x_\beta}+\rho g\frac{\partial z}{\partial x_\beta}\right)\right)=Q \qquad (1)$$

$$\alpha=\beta=1,2,3$$

where S is the storage in (m/Pa), p is the pressure in (Pa), k is the intrinsic permeability in (m²), μ is the dynamic viscosity in (Ns/m²), ρ is the density in (kg/m³), g is the gravity constant (N/s²), z is the height above a datum (m) and Q is the flow rate (m³/s) for a unit area. The discretization and solution of (1) using the finite-element method is illustrated by Istok (1989), or Kolditz (2002). Solving (1) provides the pressure heads at each node in the finite element model, which then can be interpolated for the elements and converted into flow velocities in the elements. The flow velocities v (m/s) are then used to derive the solution of the transport equation (2) Kolditz (2002), McDermott (2003) for heat flow where c is the specific heat (kJ°K^{-1}kg^{-1}) of the saturated porous rock, c^w is the specific heat of the fluid, D is the heat diffusion dispersion tensor of the porous medium (kJ°K^{-1}m^{-1}s^{-1}), T is the temperature

(°K), ρ^w is the fluid density (kg/m³), ρ is the density of the saturated porous rock.

$$c\rho\frac{\partial T}{\partial t} = D_x\frac{\partial^2 T}{\partial x^2} + D_y\frac{\partial^2 T}{\partial y^2} + D_z\frac{\partial^2 T}{\partial z^2} - c^w\rho^w v_x\frac{\partial T}{\partial x} - c^w\rho^w v_y\frac{\partial T}{\partial y} - c^w\rho^w v_z\frac{\partial T}{\partial z} - \rho Q_T \quad (2)$$

Here the heat diffusion dispersion tensor contains a component for pure diffusion, and a component for dispersion due to advection.

$$D_\alpha = D_e + v_\alpha\beta \quad (3)$$

where D_α is the heat diffusion dispersion coefficient in the α direction (kJ°K^{-1}m^{-1}s^{-1}), D_e is the effective heat diffusion coefficient (kJ°K^{-1}m^{-1}s^{-1}) (Marsily (1986)), v_α is the advective flow velocity in the α direction (m/s) and β is the heat dispersion coefficient (kJ°C $^{-1}$m $^{-2}$).

For both equations (1) and (2), the parameters of the fluid passing through the "Hot Dry Rock" and the mechanical parameters of the rock play decisive roles in the heat removal from the system. Mechanical deformation as a consequence of effective stress changes due to hydraulic injection pressures and changes in thermal stress are included in the solution of the above two equations by relating the effective stress to rock parameters via a geomechanical model. Here we consider first the pressure, temperature and salinity dependent fluid parameters secondly the hydraulic dependent rock parameters and thirdly the parameters dependent on thermal stress.

3.2 Fluid Parameters: Pressure, Temperature and Salinity Dependent

The properties of natural geo-fluids (usually saline) and injected fluids play a key role in HDR investigative and operational technology. Experimentally the hydraulic and tracer investigation of the in situ fracture system via, for instance, push-pull tests, (McDermott and Kolditz (2004), Herfort and Sauter (2003), Meigs and Beauheim (2001-05-01)) and the interpretation of the results requires an accurate understanding of the properties of the fluids under the in situ conditions. In terms of HDR plant operation, the fluids are used to transport the heat energy from the geothermal reservoir to some sort of above surface usage, e.g. electrical generation, heat supply etc. Understanding the impact and effect of changing fluid properties as a result of complex coupled processes and their influence on the rest of the system is vital in terms of predicting the short and long term behavior of geothermal reservoirs.

Figure 3 presents a plot of the systems using geothermal energy in Germany (2004). Here the operating temperature and pressure of the reservoirs are plotted on a water-vapour phase diagram. The data is taken from Kreuter and Gottlieb (2002). All the reservoirs plot in the non supercritical region. Watanabe et al. (2000) showed that the equations to calculate fluid properties as functions of pressure and temperature are extremely complicated, and investigated the changes due to temperature and pressure in supercritical geothermal reservoirs using the JSME Steam table in SI, 1980. The super critical equation of state EOS1sc was developed for TOUGH2 by Brikowiski (2001). However, supercritical conditions are not reached in potential HDR geothermal reservoirs. Significant changes are seen, however, in the fluid properties of these non supercritical reservoirs and must be taken into account when modeling heat transport. Changes of the in situ temperature and pressure are found to have a significant effect on the fluid parameters and in turn on the selection of economic energy extraction schemes, related to management of the reservoirs. Here we consider density, viscosity, specific heat capacity and heat conductivity alterations, and later examine the effects on the overall reservoir extraction scheme.

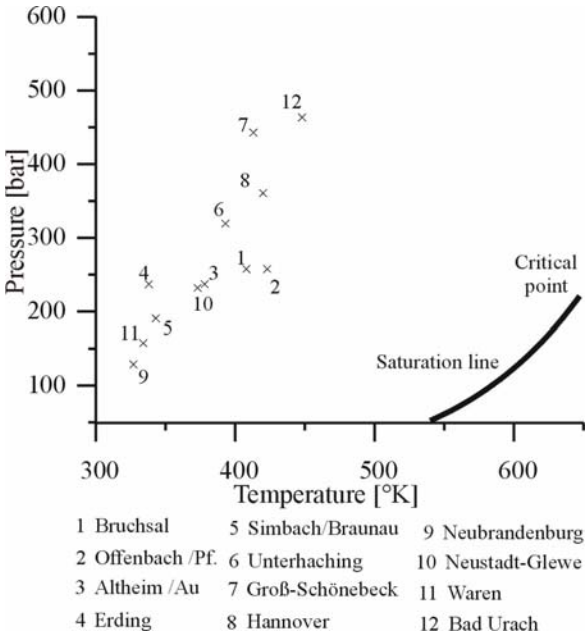

Figure 3: Temperature and pressure conditions of operational and proposed geothermal schemes in Germany.

3.2.1 Density

Fluid density is a fundamental parameter in both hydraulic flow (1) and heat transport (2). Saline water density (typical geo-fluids) is a non-linear function of salt content, temperature and pressure (Figure 4). Typically saline fluid density increases with pressure and salinity, but it decreases with increasing temperature. The effect of pressure change is smaller than the influence of variations in temperature and salt concentration Changes in density influence the flow by natural convection (density driven flow). Wagner and Kurse (1998) published formulations for density for the International Association for the Properties of Water and Steam (IAPWS). These are given below.

$$\rho(\psi,\tau) = \frac{R.T}{P}\psi\gamma_\psi \quad (4)$$

where:

$$\psi = P/P^*,\ \tau = T^*/T$$

with P* =16.53 MPa, T* =1386 K, R = 0.461526 KJ/(KgK)

and:

$$\gamma_\psi = \sum_{i=1}^{34} -n_i l_i (7.1-\psi)^{li-1}(\tau-1.222)^{Ji}$$

Here R is the gas constant, T is the temperature, P is the pressure, ψ and τ the reduced pressure and inverse

reduced temperature respectively. The remaining coefficients for these formulae may be found in the appendix.

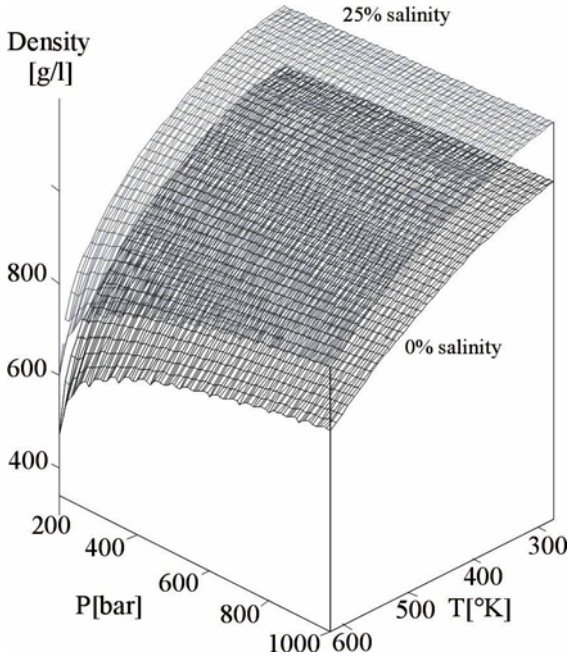

Figure 4: Variation of saline water density for non supercritical conditions as a function of pressure, temperature and salinity.

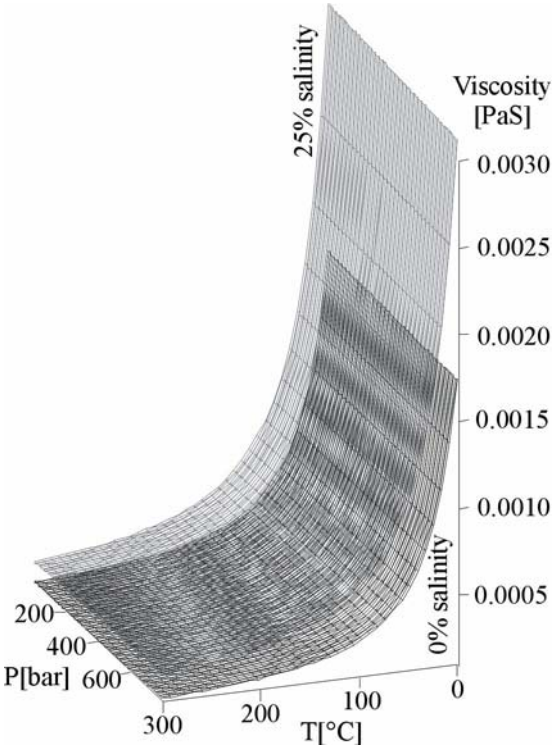

Figure 5: Variation of saline water viscosity for non supercritical conditions as a function of pressure, temperature and salinity.

3.2.2 Dynamic viscosity

Viscosity is a fundamental parameter in the calculation of hydraulic flow (1), and flow velocity (2). Fluid viscosity is strongly dependent on temperature and, to a lesser extent, on pressure and solute concentration Kenneth and Kipp (1997). The effect of pressure change on dynamic viscosity is negligible compared with salinity and temperature. Wagner and Kurse (1998) published formulations for the viscosity of water dependent on temperature and pressure for given pressure and temperature ranges. The coefficients may be found in the appendix.

$$\mu = \mu^* . \exp[\delta \sum_{i=1}^{19} n_i (\delta - 1)^{Ii} (\tau - 1)^{Ji_i}] \quad (5)$$

An empirical equation for the viscosity of water as a function of pressure, temperature, and solute concentration was adapted from a set of calculator programs for petroleum fluids, published by Hewlett-Packard (1985).

$$\mu(P,T,W_p) = \mu_0(P,T)[1 - 1.87\times10^{-3} W_P^{0.5} + 2.18\times10 - 4W_P^{2.5} + [T^{0.5} - 0.0135T][2.76\times10^{-3} W_P - 3.44\times10^{-4} W_P^{1.5}]] \quad (6)$$

with:

$$\mu_0(P,T) = 243.18\times10^{-7} \times 10^{[247.8/(T'-140)]} \times [1 + (P' - P'_{sat})1.0467\times10^{-6}(T' - 305)] \quad (7)$$

where μ_0 is the dynamic viscosity of pure water (Pas), P´ is the pressure (bar), P'_{sat} is the saturation pressure (bar), T' is the temperature (K), W_p is the weight percent of sodium chloride (%), T is the temperature (F). Figure 5 illustrates the dependency of viscosity on pressure, temperature and salinity used in the simulations.

3.2.3 Specific Heat Capacity

The specific heat capacity (c) of a fluid or rock is a measure of how much energy a unit mass of that material holds per degree (Kelvin) change in temperature ($J°K^{-1}kg^{-1}$). Comparative to fluid flow, it can be seen as relative to the storage of energy in the system. The amount of energy the geo-fluid can contain as it passes through the natural heat exchanger provided by the fracture system is an important parameter. Watanabe et al. (2000) showed that the heat capacity dramatically increases near the critical point. This means the closer the geo-fluid is to the critical point the more energy the geo-fluid can carry out of the system. Wagner and Kurse (1998) published the following formulation for isobaric specific heat capacity, here for non critical conditions

$$C_p(\psi,\tau) = -R \cdot \tau^2 \gamma_{\tau\tau} \quad (8)$$

with $\gamma_{\tau\tau} = \sum_{i=1}^{34} n_i (7.1 - \psi)^{li} Ji(Ji - 1)(\tau - 1.222)^{Ji-2}$

The coefficients are for this formula are given in the appendix.

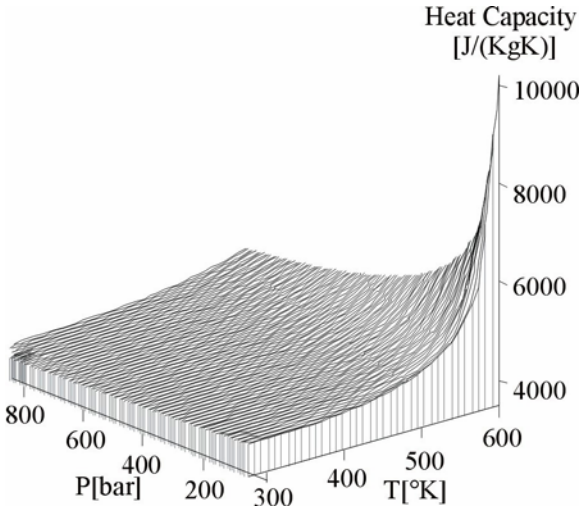

Figure 6: Variation of saline water specific heat capacity for non supercritical conditions as a function of pressure and temperature.

3.2.4 Thermal Conductivity

Thermal conductivity is defined as

$$\lambda = \rho c_p D \tag{9}$$

where the units are (W/m²), ρ is the density of the material (kg/m³) c_p is the isobaric specific heat capacity ($J°K^{-1}kg^{-1}$) and D is the thermal diffusivity ($J°K^{-1}m^{-1}s^{-1}$). Thermal conductivity is indirectly apparent in (2) with the thermal dispersivity being directly proportional to it (9). Wagner and Kurse (1998) published the an expression for the calculation of the thermal conductivity of water dependent on pressure and temperature, given in the appendix. The thermal conductivities dependence on viscosity makes it dependent on salinity as well as pressure and temperature.

Figure 7 illustrates that the geo-fluid thermal conductivity increases with pressure. At constant pressure, it increases with temperature until it reaches a maximum value at about 423°K (150 °C) after which a decrease is observed as temperature further increases. Salinity reduces the water thermal conductivity but its effect is not significant compared with pressure and temperature effects .

3.3 Solid Parameters Dependent on Pressure and Temperature

The structure of the rock and the fracture systems in the rock determines the permeability, storage and flow paths of crystalline rock system. The flow, transport and heat transport is controlled by a number of critical factors, in particular the geometry of the system in terms of the orientation of the fractures in the pervasive stress system (eg. Kessels (2000)), the fracture connectivity (Bour and Davy (1998), Manzocchi (2002-09-05)), fracture permeability (Nicholl and Detwiler (2001), Wang et al. (1988)), porosity (Montemagno and Pyrak-Nolte (1995)) and area of fracture system available for sorption and heat exchange (Renner and Sauter (1997), Wels et al. (1996), Watanabe and Takahashi (1995)). A further important aspect highlighted by a number of authors in the development of long term behavior of fracture systems is their response to stress changes generated due to hydraulic alterations of the systems, long term stress field alterations, and thermo-elastic stress alterations due to a change in the amount of heat in the systems.

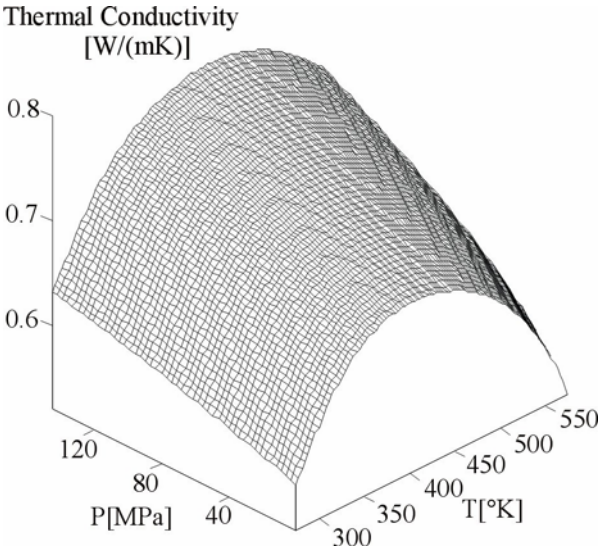

Figure 7: Variation of saline water thermal conductivity for non supercritical conditions as a function of pressure, temperature and salinity (at 1 weight percent salt content).

The response of a fracture network to stimulation by either extraction or injection of fluid is a time dependent integral signal comprising the individual responses of the discrete fractures, e.g. McDermott et al. (2003). The individual responses of the discrete fractures within the fracture system are determined by interaction of the fluid injected or extracted and its physical characteristics. Within the solid medium factors such as the elastic response of the medium and pervasive in situ conditions including temperature and pressure have a critical impact. Alterations to the contact area of the fractures, storage, effective porosity, flow channeling and permeability within the fracture system can be expected with alterations to the pervasive conditions.

The choice of model to represent the system needs to be related to the flow geometry of the system and the real flow paths available. Fracture logs indicate a fracture frequency of at least 1 fracture per meter. Sanyal et al. (2000) indicates after Pruess (1990) that where a fracture frequency of greater than around one fracture every 2-3m exists, a three-dimensional equivalent medium model of the reservoir system can be a satisfactory first approximation. We assume thermal equilibrium between the rock and the advective fluid at this stage. Included in this equivalent medium model is a discrete geomechanical approach to the changes of fracture permeability as a result of changes in effective stress during injection and extraction of fluids from this system.

In situ field tests provided information about the static permeability and storage of the reservoir system. Q-con (2003) suggest that the reservoir can be characterized with an in situ transmissivity of 0.2mD based on hydraulic investigation of the site. A personal communication from Herr Tenzer (June 2004) indicated that the transmissivity of the reservoir due to stimulation may have increased to 0.3mD. In our modeling of the longer term heat extraction characteristics of the reservoir we consider first a static permeability distribution, i.e. not pressure dependent, and secondly a dynamic permeability distribution in the reservoir, i.e. pressure dependent permeability.

As a first approximation an internal heat source for the reservoir and a conductive heat source outside of the geometrically described area of the reservoir was ignored.

Berktold et al. (1982) presented a heat flux value of around 86mWm^{-2} as typical of the Urach area. Applying this to the geometrical area of the reservoir, we get a total heat flux of some 20,000W, this compares to a recovered thermal flux by the HDR operation of a few megawatt, i.e. the natural heat flux represents less than 1% of the energy in the system, and the energy by the HDR operation is principally stored energy. Secondly the external boundaries of the reservoir were not considered to be heat conducting, in reality some extra heat can be expected to enter the reservoir from the boundaries, but by conduction only. A more complex consideration of the boundary conditions would have increased the computation time significantly. For a thirty year prediction of the reservoir behaviour including all the variable parameters, around 10 days computation was required on a Pentium 4, 3GHZ processor. Inclusion of more complicated boundary conditions and heat sources would not have significantly improved the predictive modelling, but would have increased the computation time significantly.

3.3.1 k_x, k_y, k_z Interpretation

Examining the geometry of the reservoir (Figure 1) we see that along the length of the reservoir the zone of stimulation reached some 800+m and transverse and longitudinal to the reservoir the zone of stimulation was some 300m as per the interpreted geometry of the reservoir presented in Figure 2. We interpret the difference in the length of location of stimulation to be related to anisotropy in the permeability field. The apparent homogeneous permeability over reservoir thickness of around 250m is

$$k = \frac{T}{z} = \frac{0.25miD}{250m} \approx 1e^{-15}m^2 \quad (10)$$

Where T is the measured transmissivity (mD m), and z is the thickness of the reservoir (m). Allowing *k* to represent the equivalent permeability tensor comprising a component in the x,y and z directions, where x is the long axis of the ellipsoid, z is depth and y is the lateral extent (Figure 2) the directional permeability's consistent with the in situ stress field can be calculated.

$$k^2 = k_x{}^2 + k_y{}^2 + k_z{}^2 \quad (11)$$

From the geometrical relationship, we see that in a time t, the ellipsoid had grown 800m along the x axis direction and 300m in the y and z direction. Therefore

$$k_y = k_z = \frac{3}{8}k_x \quad (12)$$

Solving (10) and (12) we derive the directional permeabilities, given in Table 1.

As the reservoir in Urach is crystalline, the permeability's are a consequence of flow in the fractures, controlled principally by the aperture of the fractures. Tenzer et al. (2004) give the measured fracture widths in the reservoir to be 0.1mm to 10mm. Applying the fracture density of around 1 fracture per m for the system we can calculate the aperture of the fractures required to produce the permeability measured. Taking the value of permeability in the x direction we can calculate what the discrete fracture opening must be to provide the measured flow rate.

$$Q = A\frac{k_f}{\mu}i \quad \text{(Darcy's law)} \quad (13)$$

$$k_f = \frac{e^2}{12} \quad \text{(Intrinsic permeability of a fracture)} \quad (14)$$

Considering Equation (13) for one fracture in a 1x1m² block, the cross sectional area of fracture involved in flow is given by $A_f = 1 \times e(m^2)$, converting this to an equivalent medium where we consider the flow in a 1 x 1m² surface, $A_{eq} = 1 \times 1(m^2)$, in accordance with Witherspoon et al. 1980 we can equate these flow rates (15) and define (16).

$$Q = \frac{e^2}{12\mu}A_f i = \frac{k}{\mu}iA_{eq} \quad (15)$$

$$\text{So } \frac{e^3}{12} = k \quad (16)$$

From (16) we can calculate the fracture aperture required to provide the equivalent permeability observed as around 0.03mm. The difference between the observed field values (0.1mm to 10mm) and the calculated is interpreted by the authors to be a consequence of the fracture geometry, and the fact that the constricted areas in the fracture dominate its permeability when measured by inducing hydraulic flow and not the wide open areas. This is expressed hydrogeologically in terms of the harmonic mean of permeability's, Baraka-Lokmane et al. (2003), and illustrated conceptually in Figure 8 for a fracture system comprising several fracture planes. For the modeling the calculated permeabilities were taken. The equivalent porosity was set equal to the observed fracture aperture, at 0.005% (5mm / m). this effects the advective velocity of the fluid in the system, but not the amount of fluid passing through the system and therefore does not effect the rate of energy removal of the system assuming equilibrium conditions within the reservoir are maintained.

Table 1: Model Parameters

Temperature of Rock	147°C
Temperature of Injected Fluid	50°C
Fluid Salinity	60g/l
Rock Matrix Density	2.85 kg/m³
Rock Matrix Conductivity	3.2Wm^{-1}K^{-1}
Heat dispersion tensor	0.01m
Permeability of Reservoir	k_x=1.53x10^{-15}m² k_y=0.57x10^{-15}m² k_z=0.57x10^{-15}m²
Ratio of Permeabilities (Geomechancial Model)	k_x=1.0 k_y=0.375 k_z=0.375
Effective Fracture Aperture at 16MPa	0.0264mm
Storage of Rock Matrix	1x10-^{10}m/Pa
Porosity of Reservoir	0.01%
Injection Pressure	+10 MPa
Extraction Pressure	-10 MPa
Fluid Viscosity	*f(Temp.,Pres.,Salinity.)*
Fluid Density	*f(Temp.,Pres.,Salinity.)*
Fluid Heat Conductivity	*f(Temp.,Pres.,Salinity.)*
Fluid Specific Heat	*f(Temp.,Pres.,Salinity.)*

3.3.2 Geomechanical Influence

Once the average aperture of a fracture responsible for defining the flow rate in the reservoir has been defined, the geomechancical response of the system can be addressed. After Tenzer et al. (2004) the maximum horizontal stress is orientated 170°N, i.e. approximately north south.

Interpreting from Tenzer (1997) the size of the total stresses within the boreholes can be given by (17)

$$\sigma_H = 0.033z$$
$$\sigma_h = 0.0144z \quad (17)$$
$$\sigma_v = 0.0266z$$

where depth (z) is in meters and the stresses are given in MPa. As the orientation of the fracture system in the reservoir between 3750m and 4445m Tenzer et al. (2004) is sub-vertical and approximately north south, we can take the minor horizontal stress, σ_h as being the total normal stress across the fractures dominating flow. It is interesting to note the geometry of the reservoir, and its correspondence to the in situ stress system, i.e. the largest permeability corresponds to the direction normal to the minimum principal stress. McDermott and Kolditz (2004) presented a geomechanical model predicting fracture aperture as a result of changes of effective stress σ', given in (18) where u is the fluid pressure in the fracture.

$$\sigma' = \sigma_h - u \quad (18)$$

This model was calibrated for the Deep Continental Borehole (KTB) site, Windeseschenbach, South East Germany, and is applied here for the derivation of the pressure dependent fracture parameters. Figure 9 illustrates the fit of the geomechanical model data with experimental data from the KTB site on a fractured sample taken from around 38000m, and the predicted behavior of the fracture system at Urach. Here the only significant difference between the two fracture systems is the elastic modulus, given from fracture logs at around 85GPa in Urach, and from field geophysics in the KTB site at around 110Gpa

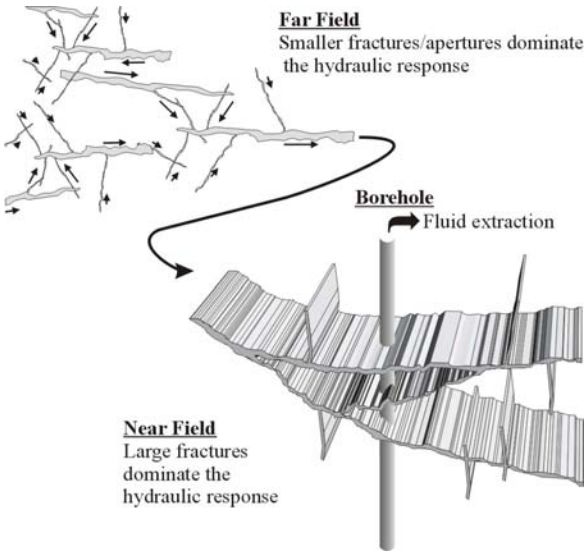

Figure 8: Hydraulic response is dominated by the smaller apertures in the fractures.

The "fracture permeability", here k_d, given by Durham (1997) in his Figure 2 refers to "the fracture permeabilities for producing the same water flux in the same pressure gradient." distributed through the bulk of the sample. The relationship between the aperture of the fracture and the k_d is given by:

$$k_d = \frac{2e^3}{12\pi r}\mu \quad (19)$$

where r is the radius of the sample being investigated.

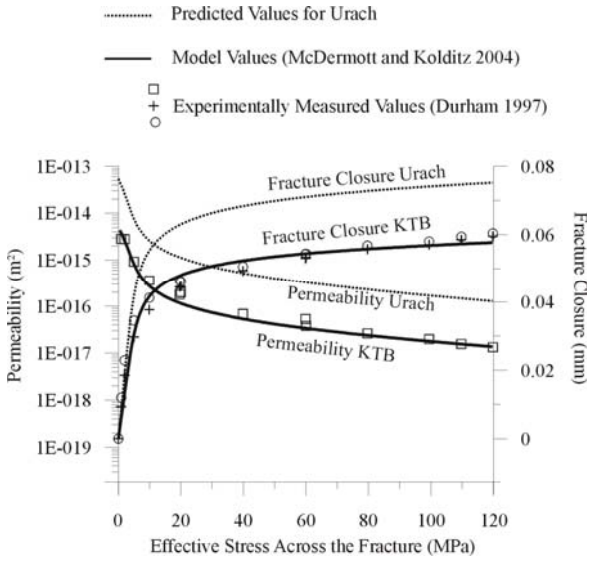

Figure 9: Relationship between the effective stress and the permeability, comparison to Durham's experimental values 1997.

3.3.3 Application of the Geomechanical Model

The effective fracture aperture dominating the hydraulic response of the system is given in Table 1 as 0.0264mm. Assuming that this value was determined for hydraulic tests in the fractured system for a normal effective stress of around 16MPa, the pressure dependent permeability characteristics of the fractured system can be estimated, as illustrated in Figure 10.

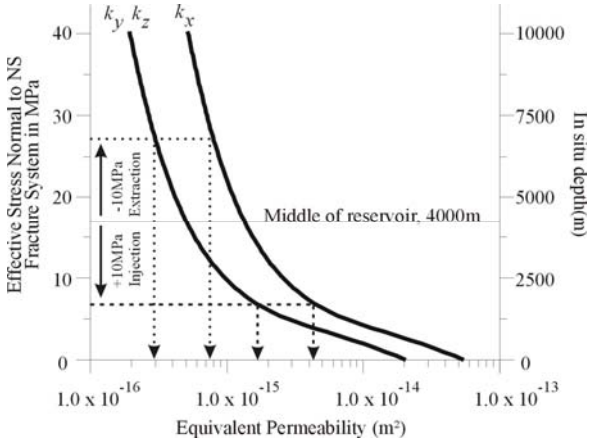

Figure 10: Equivalent permeability as a function of effective stress for Urach.

The permeability in the x direction, k_x, is calculated according to Figure 10 related to the dynamic effective stress in the model. The values k_y and k_z are calculated according to the ratio to k_x given in (12).

3.3.4 Inclusion of Thermal Stress

The thermal stress, σ_t, induced in a rock due to thermal cooling can be approximated by (20) assuming no viscous flow in the rock

$$\sigma_t = K_r E \alpha \Delta T \quad (20)$$

Here K_r is the coefficient of restraint (dimensionless), E is the elastic modulus (Pa), α is the thermal coefficient of expansion (K^{-1}) and ΔT the change in temperature in the system. The average value of the thermal coefficient of expansion for basic rocks is bassed on some 50 measurements is given by JNC (1999) as 0.82 x 10^{-5} K^{-1}. The coefficient of restraint, K_r, has a value of 1 in fully restrained systems where no movement is possible, and where movement is possible its value drops rapidly. The thermal stress is assumed to work in an opposite direction to the tectonic normal stress. This is illustrated in Figure 11.

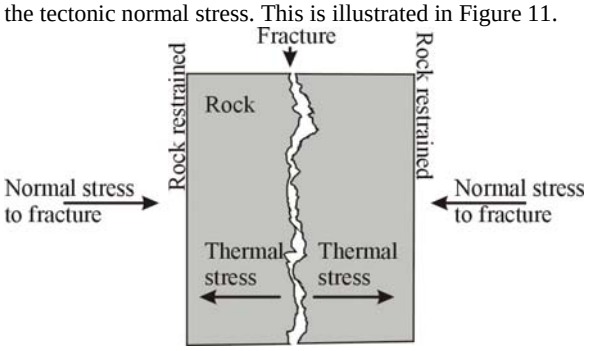

Figure 11: Consideration of thermal stress.

The effective stress across the fracture relating to Figure 10 is then given by

$$\sigma' = \sigma_h - (u + \sigma_t) \tag{21}$$

The restraint to thermal contraction and the development of the thermal stresses is dependent on the complex geometry of the rock fractures within the rock mass. Characterisation of rock mass characteristics is notoriously difficult e.g. Barton and Bandis (1990) , Bieniawski (1989), Laubscher (1977) and in all natural fracture systems movement is possible. For modeling comparison later we vary the value of K_r to investigate the effects of the thermal stress on the system.

3.4 Model Application

The effects of the coupled parameters on the extraction of heat from the reservoir and the dynamic reservoir characteristics were considered in four sets:-

- constant fluid properties and no geomechanical response to the stress alteration.
- variable fluid properties and no geomechanical response to the stress alteration.
- variable fluid properties and geomechanical response to the hydraulic stress alteration.
- variable fluid properties and geomechanical response to the hydraulic and thermal stress alteration.

Figure 12 illustrates the four principal case studies in terms of reservoir performance, three values for the coefficient of restraint are selected for the thermal impact.

3.5 Fluid Parameter Effects Only

The HDR operating conditions range from 50°C injection temperature at around 50MPa (effective normal stress across the fractures around 7MPa) to around 160°C at around 30MPa (effective normal stress across the fractures around 27MPa) extraction pressure. Considering the fluid parameters illustrated in Figures 4 through to 7, it can be seen that the most significant variation in parameters occurs with the viscosity within these temperature and pressure ranges. This is reflected in the pressure distribution within the hydraulic model. As the rock is cooled so the viscosity of the geofluid used to extract the heat from the system increases. Figure 12 illustrates the difference in the hydraulic pressure distribution between the initial pressure field and after an 8 year period of operation due to the influence of the variable fluid parameters. Here the extraction rate is approximately 21 l/s. What is of interest is that with further cooling of the reservoir, the viscosity across the reservoir becomes more consistent and the pressure distribution slowly returns to the initial field state. We should note that this is of more than just academic interest, in that the effective normal stress across the fractures controlling the permeability of the fracture system is directly dependent on the fluid pressure in the fractures, and this therefore effects the flow rates developed in the system. In Figure 12 the predicted drop in performance of the reservoir in case 2 is primarily due to the coupling of the viscosity with the flow velocity (13).

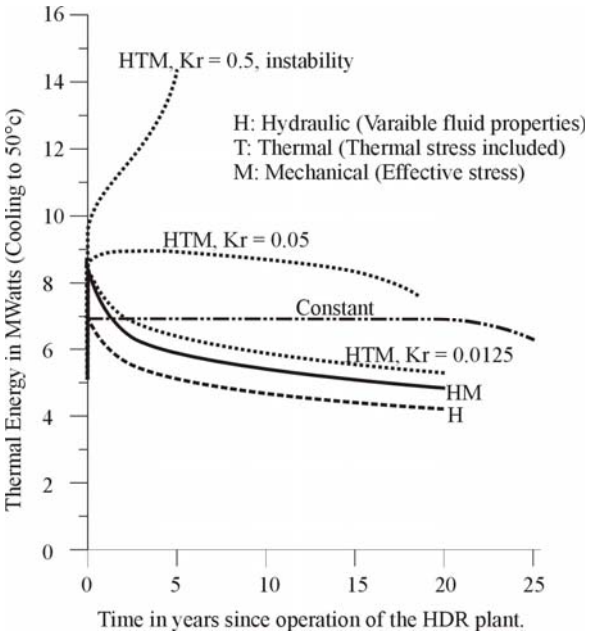

Figure 12: Reservoir long performance for constant injection and extraction pressures of +/- 10MPa.

3.6 Hydraulic Geomechanical Effects.

The amount of effective stress normal to the fracture is indirectly proportional to the fracture aperture and therefore the potential flow rate through the fracture system. The total stress normal to the dominant fractures is given by Equation (17). Considering Figure 10, we can predict that there is a around 10% difference in the permeability of along the vertical profile of the reservoir, permeability decreasing with depth. Additionally during HDR operation we inject and extract fluid at high pressures in the system, also effecting the fracture aperture and permeability, again illustrated in Figure 10 for an injection and extraction of 10MPa. Combining these effects we can state that the geomechanical model predicts a raised permeability in the vicinity of the injection borehole and a reduced permeability in the vicinity of the extraction borehole, and a vertical differentiation from higher permeability to lower permeability throughout the reservoir as a whole. In principle we can expect that the upper part of the reservoir

will carry more fluid in response to the pressure signal than the lower part of the reservoir, and therefore will exhibit more rapid cooling. The advance of the cooling front taking into account the geomechanical coupling is compared against the cooling front for the model where only the fluid parameter coupling is considered in Figure 14. Here the temperature difference between the two models is presented after 11 years for a similar overall flow rate. This figure illustrates preferential flow in the upper part of the reservoir, and reminds us also that we are dealing with a dipole system in a closed environment, and that there is hydraulic flow around the boundaries of the reservoir, leading also to changes in temperature "behind" the wells. The effect o the reservoir performance is a slight increase in the overall flow rate through the system, reflected in in an increase of thermal energy gained from the system per second.

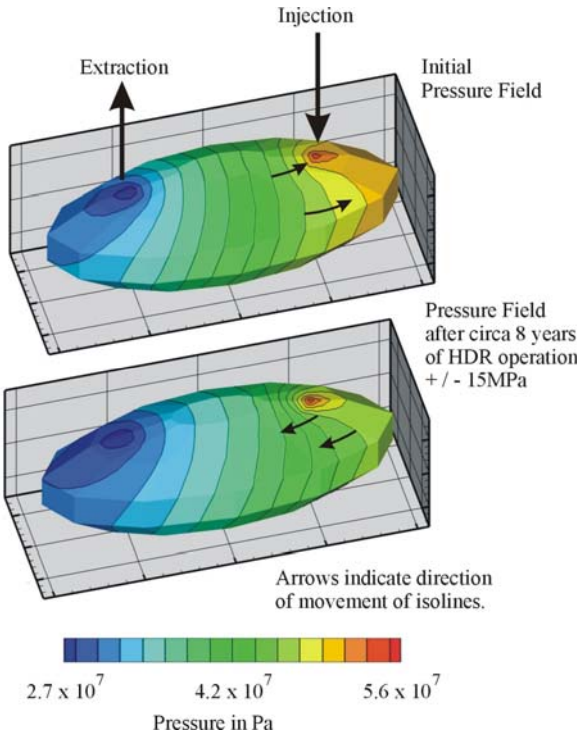

Figure 13: Hydraulic pressure and fluid parameter coupling.

3.7 Thermal Geomechanical Effects

As the temperature cold front advances in the reservoir, so the rock experiences thermal contraction. The effect of the thermal contraction is related to the permeability in the system as discussed earlier. With increasing thermal contraction, there is an increase in the size of the fracture apertures due to a reduction in the normal effective stress across the fractures and an increase in the permeability of the system. This then increases the quantity of fluid passing through the reservoir as the injection and extraction pressures are held constant and therefore the rate of heat extraction is also increased. The degree to which the thermal contraction affects the permeability is related to the mechanical restraint in the system. Three cases are presented for differing degrees of restraint related to the rock mass geometry. In each case the effect is an increase in the flow rate and rate of heat extraction from the system. For the case where Kr = 0.5 the increase in permeability in the system lead to instability in the calculations related to the finite element mesh. This is solvable by remodeling the system with a finer mesh and different time step, the consequence would be an increase in the length of calculation required.

The general result that consideration of thermal stress leads to an increase in the system permeability can be seen to be confirmed by most recent results from the KTB site. Here large volumes of cold water have been injected into the borehole with the subsequent effect that the temperature at the base of the borehole has dropped by 60°C. Concurrently it was observed that the pressure required to maintain a steady rate of injection also dropped, indicating an increase in the conductivity of the system (Personal communication Prof. Erzinger, GFZ. Potsdam, Germany, July 2004).

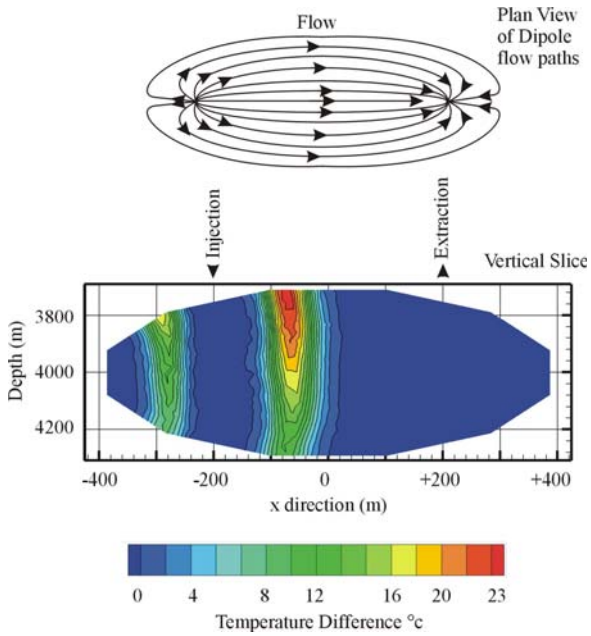

Figure 14: Influence of geomechanical coupling on the reservoir cooling in the dipole flow field. Note the increased difference towards the top of the reservoir.

3.8 Confirmation of Results

A simple calculation allows us to confirm that the results predicted by the modeling are in line with the degree of cooling expected in reality. Assuming a constant extraction rate of 21 l/s over 30 years equating to 8.4 MWatts, the amount of heat energy removed from the system can be calculated, and thereby the amount of cooling expected in the rock mass. It can be shown that a rock cube with side length of some 305m x 305m x 305m would have to be cooled by around 100°C to produce the thermal energy gained.

4. DISCUSSION OF RESERVOIR PRODUCTIVITY

At this stage the geomechanical predictions are tentative, and the modeling results need further field and experimental investigation, particularly with consideration of thermal stress release. However the results can be used to start to consider the flow and transport of heat within the reservoir and productivity.

It has been shown that to model the reservoir accurately the coupled effects of hydraulic, thermal and mechanical processes need to be taken into account. The modeling has provided a basis for the estimation of the longer term productivity characteristics of the Urach HDR site.

In terms of geometry, effectively the worst case for the reservoir was assumed, i.e. a smaller stimulated area, and no heat flow from external sources. In reality it can be expected that the reservoir is somewhat larger with potential heat flux

as well as internal heat generation. The heat resources are therefore greater than estimated.

Figure 12 presented the different effects of the various processes considered, an provides a broad range within which the reservoir is expected to respond. Further research is needed particularly into the thermo-mechanical effects.

5. CONCLUSIONS

A finite element model is presented of the HDR reservoir for Bad Urach, South West Germany.

The model is based on geophysical and geoseismic investigations, coupled with several multidisciplinary reports on the site. The reservoir is simulated using a tetrahedral meshing approximation of the major flow structure, idealized as an ellipsoid with length of 800m, and height and width of 300m.

State of the art pressure, temperature and salinity dependent functions for the calculation of the fluid parameters coupled with a geomechanical model combining mechanical and thermal deformation (HTM) were incorporated to enable initial estimations of the productivity and operational life of the reservoir. The effects of the different processes on the reservoir characteristics were investigated.

As a first approximation of the system, the model provides information regarding the potential long term productivity of the system, and points to areas which need urgent further consideration and experimental investigation, particularly related to the consideration of the effects of thermal stress release in the system and the development of preferential flow paths.

AKNOWLEDGEMENTS

We thank the Federal Ministry of the Environment, Nature Conservation and Nuclear Safety of Germany (BMU) and the German Science Foundation (DFG) for funding. In addition we thank the city of Bad Urach geothermal research group and the company Q-con for seismic and hydraulic data. Finally the authors gratefully acknowledge the work of Geo-Forschungs Zentrum (GFZ), Potsdam regarding the use of data and information pertaining to the KTB site.

REFERENCES

Baisch, S., R. Weidler, R. Voeroes, H. Tenzer and D. Teza (2004). Improving hydraulic simulation efficiency by means of real time monitoring. Proceedings of the 29th Workshop on Geothermal Reservoir Engineering, Stanford University, Stanford, California.

Baraka-Lokmane, S., R. Liedl and G. Teutsch (2003). "Comparison of Measured and Modelled Hydraulic Conductivites of Fractured Sandstone Cores." Pure and Applied Geophysics 160: 909-927.

Barton, N. and S. Bandis (1990). Review of Predictive Capabilities of JRC-JCS Model in Engineering Practice. Proc. Int. Symp. on Rock Joints, (Leon, June 4-6, 1990), A.A. Balkema.

Berktold, A., R. Haenel and J. Wohlenberg (1982). A model of the Urach geothermal anaomaly as derived from geophysical investigations. The Urach Geothermal Project (Swabain Alb, Germany. R. Haenel, E. Schweizerbart'sche Verlagsbuchhandlung (Nägele u. Obermiller), Stuttgart: 401-411.

Bieniawski, Z. T. (1989). Engineering Rock Mass Classification, New York: John Wiley & Sons

Bour, O. and P. Davy (1998). "On the connectivity of three-dimensional fault networks." Water Resour. Res. 34(10): 2611 - 2622.

Brikowiski, T. H. (2001). Modeling supercritical systems with TOUGH2: Prememinary results using EOS1sc equation of state module. Proceedings of the 26th Workshop on Geothermal Reservoir Engineering, Stanford University, Stanford, California.

Diersch, H. J. (1985). Modellierung und numerische Simulation geohydrodynamischer Transportprozesse. Akademie der Wissenschaften der DDR. Berlin: 267.

Durham, W. B. (1997). "Laboratory observations of the hydraulic behavior of a permeable fracture from 3800 m depth in the KTB pilot hole." J. Geophys. Res. 102(B8): 18405 - 18416.

Freeze, R. A. and J. A. Cherry (1979). Groundwater, Prentice Hall, Englewood Cliffs, NJ 07632.0-13-365312-9.

Haenel, R., Ed. (1982). The Urach Geothermal Project (Swabain Alb, Germany, E. Schweizerbart'sche Verlagsbuchhandlung (Nägele u. Obermiller), Stuttgart.3 510 65107 3.

Helmig, R. (1997). Multiphase flow and transport processes in the subsurface., Springer Verlag.

Herfort, M. and M. Sauter (2003). Investigation of matrix diffusion in deep hot-dry-rock reservoirs using SWIW tracer tests. Groundwater in Fractured Rocks., Prague.

Hewlett-Packard (1985). HP-41C manual, Petroleum fluids pac, Corvallis, OR

Huyakorn, P. S. and G. F. Pinder (1983). Computational methods in subsurface flow., Academic Press

Istok, J. (1989). Groundwater Modeling by the Finite Element Method, American Geophysical Union. 0-87590-317-7.

JNC (1999). Japan Nuclear Cycle Development Institute: H12 : Project to Establish the Scientific and Technical Basis for HLW Disposal in Japan, Supporting Report 1 "Geological Environment in Japan". http://www.jnc.go.jp

Kenneth, L. and J. Kipp (1997). Guide to a revised heat and solute transport simulator: HST3D-Version 2, Water Resources Investigations Report 97-4157, US Geological Survey, Denver, Colorado

Kessels, W. (2000). Elastische Eigenschaften von Klüften und Interpretation hydraulischer Tests-Untersuchungen im Rahmen des KTB - Projektes. 3. Workshop Kluft- Aquifere "Gekoppelte Prozesse in Geosystemen", Institut für Strömungsmechanik und Elektron. Rechnen im Bauwesen der Universität Hannover.

Kolditz, O. (2001). "Non-linear flow in fractured rock." International Journal of Numerical Methods for Heat & Fluid Flow 11(6): 547-575.

Kolditz, O. (2002). Computational Methods in Environmental Fluid Mechanics, Springer-Verlag Berlin Heidelberg New York

Kolditz, O. and C. Clauser (1998). "Numerical simulation of flow and heat trasferin fractured crystalline rocks: Application to the hot dry rock site in Rosemanowes (U.K.)." Geothermics 27(1): 1-23.

Kreuter, H. and J. Gottlieb (2002). Geothermische Stromerzeugung aus dem Muschelkal im Oberrheingraben: Das HorRock-Projeckt in Offenbach and der Queich. 20 Jahre Tiefe Geothermie in Deutschland: 7. Geothermische Fachtagung, Waren (Müritz), Germany, Federal Ministry of the Environment, Nature Conservation and Nuclear Saftey of Germany (BMU Public Relations Divison, D-11055 Berlin.

Laubscher, D. H. (1977). "Geomechanics Classification of Jointed Rock Masses - Minning Applications." Trans. Inst. Min. Metall. (Sect A: Min. Industry) 86: A1-A8.

Manzocchi, T. (2002-09-05). "The connectivity of two-dimensional networks of spatially correlated fractures." Water Resour. Res. 38(9).

Marsily, G. d. (1986). Quantitative Hydrogeology, Academic Press.0-12-208916-2.

McDermott, C. I. (2003). Inside Finite Elements for Outsiders; Groundwater flow, stationary and transient conditions, contaminant transport, heat transport, stress strain, Technical report, Groundwater Modelling Group, Center for Applied Geosciences, University of Tübingen. Germany

McDermott, C. I. and O. Kolditz (2004). Hydraulic-Geomechanical effective stress model: Determination of some discrete fracture network parameters from a pump test and application to geothermal reservoir modelling. Twenty-Ninth Workshop on Geothermal Reservoir Engineering, Stanford University, Stanford, California.

McDermott, C. I., M. Sauter and R. Liedl (2003). "New experimental techniques for pneumatic tomographical determination of the flow and transport parameters of highly fractured porous rock samples,." Journal of Hydrology 278(1-4): 51-63.

Meigs, L. C. and R. L. Beauheim (2001). "Tracer tests in a fractured dolomite 1. Experimental design and observed tracer recoveries." Water Resour. Res. 37(5).

Montemagno, C. D. and L. J. Pyrak-Nolte (1995). "Porosity of natural fracture networks." Geophys. Res. Lett. 22(11): 1397 - 1400.

Nicholl, M. J. and R. L. Detwiler (2001). "Simulation of flow and transport in a single fracture: Macroscopic effects of underestimating local head loss." Geophys. Res. Lett. 28(23): 4355 - 4358.

O'Sullivan, M. J., K. Pruess and M. J. Lippmann (2001). "Geothermal reservoir simulation; The state of practice and emerging trends." Geothermics 30(4): 395-429.

Pham, M., C. Klein, S. Sanyal, T. Xu and K. Pruess (2001). "Reducing cost and environmental impact of geothermal power through modeling of chemical processes in the reservoir." Proceedings of the 26th Workshop on Geothermal Reservoir Engineering, Stanford University, California.

Pruess, K. (1990). "Modeling of geothermal reservoirs: fundermental processes, computer simulation, and field applications." Geothermics 19(1): 3-15.

Q-con (2003). Langzeitinjektion in der Bohrung Urach 3, SWBU007

Renner, M. and M. Sauter (1997). Heat as natural tracer: Characterization of a conduit network in a karst aquifer using temperature measurements of the spring water. Karst Waters Environmental Impacts. G. G. G and A. I. J. A. I., Balkema, Rotterdam.: 423-431.

Sanyal, S. K., S. J. Butler, D. Senson and B. Hardeman (2000). Review of the state of the art of numerical simulation of enhanced geothermal systems. Proceedings World Geothermal Congress 2000, Kyushu-Tohoku, Japan.

Sauter, M., I. Ghergut, M. Herfort and M. Lodemann (2004). "HDR Bad Urach. Teilprojekt Push-Pull-Tracer-Versuch Urach-3., Abschlussbericht, Geoscientific Center at the University of Göttingen, Georg-August University of Göttingen, Germany.

Tenzer, H. (1997). Erkundung planarer Diskontinuitäten, Bohrlochwandausbrüchen, sowie von Spannungsdaten und hydraulischen Parametern im Gneisgebirge der Vertiefungbohrung Urach 3, BEO/BMBF 0326938A, CEC JOU2 CT 92-0115, Stadtwerke Bad Urach, Marktplatz 8-9, D-72574

Tenzer, H., U. Schanz, G. Homier, H. Stang, R. Weidler and S. Baisch (2002). Weiterentwicklung, Nachweis und Demonstration standortunabhäangiger HDR-Konzeption zur Strom und Wärmegewinnung aus heißem Tiefengestein unter Berücksichtigung geologischer, hydraulischer, technischer und wirtschaftlicher Verfahrens- und Anlagenparameter für Basisdaten einer HDR-Pilotanlage. 20 Jahre Tiefe Geothermie in Deutschland: 7. Geothermische Fachtagung, Waren (Müritz), Germany, Federal Ministry of the Environment, Nature Conservation and Nuclear Saftey of Germany (BMU Public Relations Divison, D-11055 Berlin.

Tenzer, H., U. Schanz, H. Stang, G. Homier, S. Baisch, R. Weidler, A. Macek and S. Uhlig (2004). The hot dry rock project at Bad Urach. Present state and perspectives of geothermal power generation in germany. U. Bruchmann, M. Kaltschmitt and G. Schroeder, Federal Ministry of the Environment, Nature Conservation and Nuclear Saftey of Germany (BMU) Public Relations Divison, D-11055 Berlin.

Tsang, C.-F. (1991). "Coupled hydromechanical-thermochemical processes in rock fractures." Rev. Geophys. 29(4): 537 - 552.

Wagner, W. and A. Kurse (1998). Properties of water and steam: the industrial standard IAPWS-IF97 for the thermodynamic properties and supplementary equations for other properties; tables based on these equations., Berlin, Springer

Wang, J. S. Y., T. N. Narasimhan and C. H. Scholz (1988). "Aperture correlation of a fractal fracture." J. Geophys. Res. 93(B3): 2216 - 2224.

Watanabe, K., Y. Niibori and T. Hashida (2000). Numerical study on heat extraction from supercritical geothermal reservoir. Proceedings World Geothermal Congress 2000, Kyushu-Tohoku, Japan.

Watanabe, K. and H. Takahashi (1995). "Fractal geometry characterization of geothermal reservoir fracture networks." J. Geophys. Res. 100(B1): 521 - 528.

Wels, C., L. Smith and T. T. Vandergraaf (1996). "Influence of specific surface area on transport of sorbing solutes in fractures: An experimental analysis." Water Resour. Res. 32(7): 1943 - 1954.

APPENDIX

Coefficients for density, specific heat capacity,

i	l_i	J_i	n_i
1	0	-2	0.146329712
2	0	-1	-0.84548187
3	0	0	-3.76E+00
4	0	1	3.39E+00
5	0	2	-0.95791963
6	0	3	0.157720385
7	0	4	-1.66E-02
8	0	5	8.12E-04
9	1	-9	2.83E-04
10	1	-7	-6.07E-04
11	1	-1	-1.90E-02
12	1	0	-3.25E-02
13	1	1	-2.18E-02
14	1	3	-5.28E-05
15	2	-3	-4.72E-04
16	2	0	-3.00E-04
17	2	1	4.77E-05
18	2	3	-4.41E-06
19	2	17	-7.27E-16
20	3	-4	-3.17E-05
21	3	0	-2.83E-06
22	3	6	-8.52E-10
23	4	-5	-2.24E-06
24	4	-2	-6.52E-07
25	4	10	-1.43E-13
26	5	-8	-4.05E-07
27	8	-11	-1.27E-09
28	8	-6	-1.74E-10
29	21	-29	-6.88E-19
30	23	-31	1.45E-20
31	29	-38	2.63E-23
32	30	-39	-1.19E-23

$\delta = \rho / \rho^*$ with ρ^* = 317.763 Kg.m^{-3}

$\tau = T^* / T$ with T*= 1386 K

$\psi = P / P^*$ with P*= 16.53 MPa

273.15 K $\leq$ T $\leq$ 623.15 K and Psat $\leq$ P $\leq$ 100MPa
after Wagner and Kurse (1998)

Coefficients for viscosity

i	li	ji	ni
1	0	0	0.513 204 7
2	0	1	0.3205656
3	0	4	- 0.778 256 7
4	0	5	0.188 544 7
5	1	0	0.2151778
6	1	1	0.731 788 3
7	1	2	1.241044
8	1	3	1.476783
9	2	0	-0.2818107
10	2	1	-1.070786
11	2	2	-1.263184
12	3	0	0.1778064
13	3	1	0.460 504 0
14	3	2	0.234 037 9
15	3	3	- 0.492 417 9
16	4	0	-0.0417661
17	4	3	0.160 043 5
18	5	1	-0.01578386
19	6	3	-0.0036295

$\delta = \rho / \rho^*$ with ρ^* = 317.763 Kg.m^{-3}

μ^* = 55.071e-6 Pas

$\tau = T^* / T$ with T*= 647.226 K

273.15K $\leq$ T $\leq$ 423.15K and p $\leq$ 500 MPa
423.15K <T $\leq$ 873.15K and p $\leq$ 350 MPa
873.15K<T $\leq$ 1173.15K and p $\leq$ 300 MPa
after Wagner and Kurse (1998)

Coefficients for thermal conductivity λ

$\lambda = \Lambda \cdot \lambda^*$ with $\lambda^* = 0.4945$ Wm^{-1}K^{-1}

$$\Lambda(\delta,\tau) = \Lambda_0(\tau)\cdot\Lambda_1(\delta,\tau) + \Lambda_2(\delta,\tau)$$

where $\delta = \rho / \rho^*$ and $\tau = T^* / T$ with $\rho^* = 317.763$ Kg.m^{-3}
and T*= 647.226 K.

Coefficients for the calculation of $\Lambda_0(\tau)$

i	n^0_i
0	1
1	6.978267
2	2.599096
3	-0.998254

$$\Lambda_0(\tau) = \left[\tau^{0.5}\sum_{i=0}^{3} n_i^0 \tau^i\right]^{-1}$$

$$\Lambda_1(\delta,\tau) = \exp\left[\delta\sum_{i=0}^{4}\sum_{j=0}^{5} n_{ij}(\tau-1)^i(\delta-1)^j\right]$$

Coefficients for the calculation of $\Lambda_1(\delta,\tau)$

j	n_{0j}	n_{1j}	n_{2j}	n_{3j}	n_{4j}
0	1.33	1.70	5.22	8.71	-1.85
1	-0.40452437	-2.22	-1.01E+01	-9.50	0.9340469
2	0.2440949	1.65	4.99	4.38	0
3	1.87E-02	-0.76736002	-0.27297694	-0.91783782	0
4	-0.12961068	0.37283344	-0.43083393	0	0
5	4.48E-02	-0.1120316	0.13333849	0	0

$$\Lambda_2(\delta,\tau) = \frac{0.0013848}{\mu/(55.071x10^{-6})}(\tau\delta)^{-2}\left(\frac{\partial\psi}{\partial(\tau-1)}\right)_\delta^2\left[\delta\left(\frac{\partial\delta}{\partial\psi}\right)_\tau\right]^{0.4678}$$
$$\delta^{0.5}\cdot\exp\left[-18.66\cdot(\tau^{-1}-1)^2-(\delta-1)^4\right]$$

with μ being the dynamic viscosity.

$$\left(\frac{\partial\psi}{\partial(\tau-1)}\right)_\delta = \frac{\tilde{T}^* P^*(\gamma_{\psi\tau}T^* - \gamma_\psi T)}{\tilde{P}^* T^2 \gamma_{\psi\psi}}$$

$$\left(\frac{\partial\delta}{\partial\psi}\right)_\tau = -\frac{\tilde{P}^*\gamma_{\psi\psi}}{\tilde{\rho}^* RT\gamma_\psi^2}$$

$$\gamma_\psi = \sum_{i=1}^{34} -n_i l_i (7.1-\psi)^{li-1}(\tau-1.222)^{Ji}$$

$$\gamma_{\tau\tau} = \sum_{i=1}^{34} n_i (7.1-\psi)^{li} Ji(Ji-1)(\tau-1.222)^{Ji-2}$$

$$\gamma_{\psi\tau} = \sum_{i=1}^{34} -n_i l_i (7.1-\psi)^{li-1} Ji(\tau-1.222)^{Ji-1}$$

$$\gamma_{\psi\psi} = \sum_{i=1}^{34} n_i l_i (l_i-1)(7.1-\psi)^{li-2} Ji(Ji-1)(\tau-1.222)^{Ji}$$

with: $\tilde{T}^*$ = 647.226 K, $\tilde{P}^*$ = 22.115 MPa, $\tilde{\rho}^*$ = 317.763 Kg.m^{-3}
T*= 1386K, P*= 16.53MPa
Ranges of validity:
273.15K $\leq$ T $\leq$ 398.15K and p $\leq$ 400 MPa
398.15K<T $\leq$ 523.15K and p $\leq$ 200 MPa
523.15K<T $\leq$ 673.15K and p $\leq$ 150 MPa
673.15K<T $\leq$ 1073.15K and p $\leq$ 100 MPa
After Wagner and Kurse (1998)